This paper was originally published as an *ASHRAE Transactions paper* and may be cited as:

Eslami-nejad, P. and M. Bernier. 2013. A preliminary assessment on the use of phase change materials around geothermal boreholes, ASHRAE Transactions 119(2):312-321.

2013 ASHRAE Technical paper award.

DE-13-028

A Preliminary Assessment on the Use of Phase Change Materials around Geothermal Boreholes

Parham Eslami-nejad, PhD

Michel Bernier, PhD, PE
Member ASHRAE

ABSTRACT

A new borehole configuration is proposed in this study in an attempt to reduce the required length of ground heat exchangers (GHE) in cooling-dominated climates. It consists of a single U-tube borehole surrounded by a ring made of a thermally enhanced phase change material (PCM) mixed with sand.

With a properly designed PCM ring around the borehole, a significant portion of the rejected heat during peak building loads is used to melt a PCM. This slows down the increase in the return temperature to the heat pump. In nonpeak periods when the heat pump is not operating, thermal energy stored in the ring is released into the ground by heat conduction. In the process, the PCM ring solidifies and is then ready for the release of heat during the next heat pump operation cycle. By taking advantage of the relatively high energy content associated with the latent heat of fusion of PCM, the PCM ring may reduce the required borehole length. This paper presents the numerical model used to obtain the temperature distribution around the borehole and in the PCM ring. Several annual simulations were undertaken to evaluate the merits of the proposed borehole configuration in a cooling-dominated climate. Preliminary results show that the proposed configuration can reduce the borehole length by up to 9%.

INTRODUCTION

In ground source heat pump (GCHP) systems, heat is extracted from or rejected to the ground using ground heat exchangers (GHE) to provide space conditioning and domestic hot water. Vertical GHEs are most often used as they offer high-energy efficiencies due mainly to relatively constant ground temperatures. However, high drilling costs for the ground loop portion have been identified as the main barrier for widespread utilization of this technology.

When the GCHP system operates in cooling mode, it rejects heat into the ground, which increases the ground temperature near the borehole and the entering fluid temperature (EFT) to the heat pump. The required borehole length is usually determined so as to limit the EFT below safe operational limits at peak conditions. It is suggested here to use the latent heat of fusion of phase change materials (PCM) to slow down the increase in the EFT during peak conditions,

The system under study is mainly aimed at residential applications and is presented schematically in Figure 1. It consists of a single U-tube borehole connected to a heat pump. The U-tube is surrounded by grout, just like in a regular borehole. In addition, this borehole is surrounded by a relatively thin (a few centimeters) thermally enhanced PCM ring. Sand is added to the PCM ring to increase the overall conductivity of the mixture. Such a ring would certainly involve new ways of constructing boreholes, some of which are under development. This paper, however, concentrates on the modeling aspects to determine the potential of this configuration.

During peak cooling loads, the ground temperature in the vicinity of boreholes increases, which reduces the heat transfer and increases the EFT to the heat pump. Consequently, the length of the GHE has to be long enough to enable the required heat exchange and to decrease the EFT to the heat pump. With a properly designed PCM ring operating at an adequate melting temperature, a significant portion of the rejected heat during peak loads is used to melt a PCM. This slows down the increase in the EFT to the heat pump and takes advantage of the relatively high energy content associated with the latent heat of fusion of PCM. In effect, the EFT remains essentially

Parham Eslami-nejad is a postdoctoral fellow with Natural Resources Canada, Canment-Energy, Varennes, Quebec and **Michel Bernier** is a professor, Polytechnique Montreal, Montreal, Quebec, Canada.

constant during peak conditions when a PCM ring is used. In nonpeak periods, when the heat pump is not operating, the thermal energy stored in the ring is released into the ground by heat conduction. In the process, the PCM ring releases its accumulated heat, solidifies, and is ready for the release of heat from the borehole during the next heat pump operation cycle.

In this study, a 1-*D* (radial) numerical heat transfer model of the ground, developed by Eslami-nejad and Bernier (2012), is adapted and coupled to an analytical model of a single U-tube borehole (Zeng et al. 2003). The ground model accounts for the melting/solidifying process occurring in the PCM ring as well as heat transfer in the ground. It is integrated with other component models (building and heat pump) to conduct system simulations of a realistic heat pump operation to evaluate the merits of the proposed borehole configuration in a typical cooling-dominated climate. Annual simulations are performed with a 6 min. time step. Furthermore, several simulations were undertaken to evaluate the optimum PCM ring radius under specific conditions.

LITERATURE REVIEW

During the last decades, researchers have proposed different alternatives to reduce the length of boreholes including improvements to the grout and U-tube thermal properties.

Allan and Kavanaugh (1999) performed laboratory studies to measure the thermal conductivity of cementitious grouts containing different fillers. They also determined theoretically the influence of using such grouts on the borehole length. They concluded that depending on bore diameter and soil thermal conductivity, borehole length could be reduced by 22% to 37% for a 100-ton load test case compared to cement-based grout.

Another set of laboratory studies was performed by Remund (1999) to determine the effect of grout thermal conductivity, borehole diameter, pipe size, and pipe configuration on the total thermal resistance in the borehole. He reported that the borehole thermal resistance decreased by up to 19%

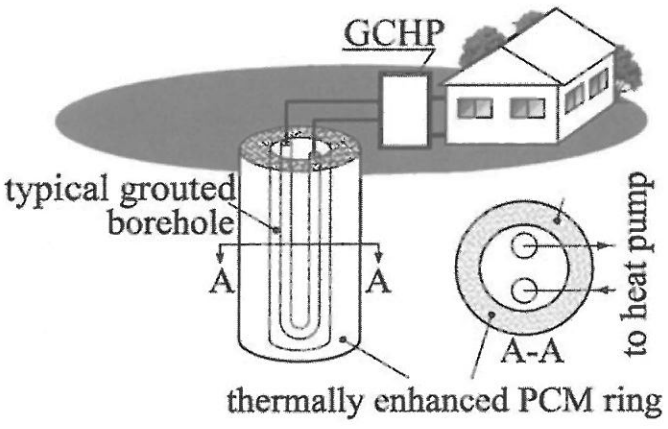

Figure 1 *Schematic representation of the system configuration.*

with increasing grout thermal conductivity, which can in turn shorten the required borehole length. However, he found that increasing grout thermal conductivity over 1.7 $W/m^{-1}\cdot K$ (0.98 $Btu\cdot h^{-1}\cdot ft^{-1}\cdot °F^{-1}$) provided very small additional reductions.

Raymond et al. (2011) performed two and three-dimensional numerical simulations to evaluate the performance of a newly developed HDPE pipe with higher thermal conductivities. Results indicated that the thermally enhanced pipe reduces the borehole thermal resistance by up to 24% for a single U-tube borehole, which shortens required borehole length by up to 9% for specific load conditions.

There are other solutions to reduce borehole length. For example, it is possible to use a supplementary source of energy or a heat rejection system at peak conditions. In such cases, the resulting systems are often referred to as hybrid GCHP systems, or simply HyGCHP systems.

For heating applications, recent studies have combined solar energy to GCHP systems to balance ground loads on an annual basis and reduce the borehole length. For example, Yang et al. (2010) and Xi et al. (2011) recently indicated that using thermal solar collectors to charge the heat pump evaporator is a feasible way to make GCHP systems attractive for space heating and domestic hot-water production in cold climates.

Kjellsson et al. (2010) reported that a hybrid system with solar heat injection into the boreholes in winter and solar domestic hot-water production during the summer is the option with the highest electrical consumption savings. Chiasson and Yavuzturk (2003) found that solar heat injection into multiple boreholes can reduce the borehole length and make the system economically viable. However, it has been shown that solar heat injection into a single-borehole does not reduce the borehole length significantly (Bernier and Shirazi 2007) and that for a fixed borehole length, the heat pump energy consumption does not change significantly (Eslami-nejad et al. 2009). Furthermore, coupling solar thermal collectors and GCHP systems using typical borehole configuration requires an extra heat exchanger, which may add to the complexity of the system and introduce a source of inefficiency in the system (Eslami-nejad and Bernier 2011a).

Recently, Eslami-nejad and Bernier (2011a, 2011b) developed a new borehole configuration with two independent U-tubes: one U-tube is linked to a heat pump and the other is connected to thermal solar collectors. With this setup, simultaneous heat injection and rejection in the borehole is possible. Eslami-nejad and Bernier (2011a) performed several multi-annual simulations to examine the impact of thermal recharging of a single-borehole using the proposed configuration. They indicated that despite a relatively large amount of solar energy injected into the borehole, the annual heat pump energy consumption is not reduced significantly. However, the proposed system might contribute to reduced installation costs as it leads to shorter boreholes. They concluded that since the available solar energy injected into the borehole is not necessarily coincident with the peak building loads, it dissipates

rapidly into the ground without making proportional effects on the required borehole length. The double U-tube borehole configuration with solar heat injection has also been used by Eslami-nejad and Bernier (2012) in a cold-climate condition. The borehole was equipped with a sand ring much like the one presented here. However, in that case the PCM is water that is mixed with the sand. Results show that the borehole wall temperature remains around 0°C (32°F) for several days when the ring freezes, while it would drop to much lower values without the saturated sand ring. When available, solar energy can melt the frozen ring and recharge the borehole for the next heat extraction cycle. They reported a reduction of up to 38% in borehole length for small thermal conductivity grounds.

For cooling applications, supplementary heat rejection devices, such as cooling towers are used to prevent heat build-up in the ground to reduce GHE length and improve system performance. A life-cycle cost study was conducted by Yavuzturk and Spitler (2000) for a small office building using an hourly system simulation to compare various operating and control strategies under two different weather conditions. They concluded that in general the HyGCHP system is beneficial on a total cost basis for relatively hot and even for moderately warm climates. However, operating and control strategies can significantly increase the total cost of the HyGCHP systems.

Chiasson and Yavuzturk (2009) optimized HyGCHP systems by minimizing the borehole heat exchanger length and appropriately sizing supplemental equipment to balance the annual thermal loads on the ground. They conducted several simulations to develop a design method for estimating the total ground-loop length in cooling-dominated buildings.

Hackel et al. (2009) identified the optimal equipment size and control strategy of HyGCHP systems for cooling-dominated conditions under different climates. A 20-year life-cycle cost analysis was conducted using a simulation model built in TRNSYS. The model was integrated with an optimization engine to develop design guidelines for the HyGCHP systems. They reported life-cycle cost savings associated with the lower first cost of the ground loop heat exchanger and more efficient operation of the HyGCHP system.

Even though the use of supplemental heat rejecters appears to be beneficial for relatively large buildings, initial costs and electricity consumption of heat rejecters may diminish the potential savings if the HyGCHP system is not carefully designed (Yavuzturk 2000). Furthermore, relatively complex operating and control strategies for HyGCHP systems have a significant influence on the system benefits.

In this paper, a new approach is presented where the supplementary heat rejecter is replaced by a PCM-sand ring around a regular grouted borehole.

MODEL

Development

A 1-*D* heat conduction model including phase change is developed in the ground, i.e., from the borehole wall to the far-field. The model accounts for melting/solidification of the PCM ring as well as heat transfer in the ground and in the PCM ring. Three phases are considered in the PCM ring: solid PCM-sand mixture, liquid PCM-sand mixture, and a transition phase. The governing equation is the energy equation (pure conduction) in cylindrical coordinates:

$$\rho c \frac{\partial T}{\partial t} = \frac{1}{r}\frac{\partial}{\partial r}\left(kr\frac{\partial T}{\partial r}\right) \tag{1}$$

where ρc is the heat capacity and k is thermal conductivity. Based on a procedure outlined by Bonacina et al. (1973), these physical properties are constant for a given phase and are given as follows:

Liquid phase (liquid PCM and sand):

$$\begin{aligned} &\text{if } T \geq T_m + \delta \\ &k = k_{is} \\ &\rho c = \rho_{sp} c_s (1-\phi) + \rho_w c_w \phi \end{aligned} \tag{2}$$

Solid phase (solid PCM and sand):

$$\begin{aligned} &\text{if } T \leq T_m - \delta \\ &k = k_{ws} \\ &\rho c = \rho_{sp} c_s (1-\phi) + \rho_w c_i \phi \end{aligned} \tag{3}$$

Transition phase:

$$\begin{aligned} &\text{if } T_m - \delta \leq T \geq T_m + \delta \\ &k = k_{is} + \frac{k_{ws} - k_{is}}{2\delta}[T - (T_m - \delta)] \\ &\rho c = \rho_{sp} c_s (1-\phi) + \rho_w \left(\frac{c_w + c_i}{2} + \frac{L}{2\delta}\right)\phi \end{aligned} \tag{4}$$

where T_m is the temperature at which the change of phase occurs, 2δ is the phase change temperature range, L is the latent heat per unit mass, and ϕ is the sand porosity. Subscripts *is* and *ws* refer to the bulk average values for the solid PCM and liquid PCM regions, respectively. For example, k_{is} is the bulk average thermal conductivity for the solid PCM-soil mixture. The remaining parameters are: ρ_{sp} and ρ_w, the densities of sand particles and PCM, respectively and c_s, c_i, and c_w, the sand, solid PCM and liquid PCM specific heats, respectively. The density of the PCM is assumed to remain constant in each phase, thus ρ_w is used for both liquid and solid states.

Equation 1 is discretized using the classic fully-implicit finite-volume approach (Patankar 1980) with Type-B grids. The resulting coupled nonlinear (properties are temperature dependent) set of algebraic equations are solved over the whole domain using the tridiagonal matrix algorithm (Patankar 1980).

In this study, the effective heat capacity is used to handle the phase change phenomenon. Consequently, the latent heat effect is approximated by a large effective specific heat over a small temperature range. The effective heat capacity approach is simple in its implementation. However, problems regarding grid independence and convergence have been reported. Solutions to these problems have been documented by Eslami-nejad and Bernier (2012).

Spatial and temporal grid independence checks have been performed. In the PCM-sand region, where phase change occurs, very fine grids of the order of 0.15 mm (0.006 in.), are required. In the ground region, 20 mm (0.75 in.) grids are used. Since the first order fully-implicit approach is used, the model is relatively stable for time steps in the 1 to 60 s range. For that interval, small differences are observed in the results. More details regarding this model are given by Eslami-nejad and Bernier (2012).

Experimental Validation

An experimental setup has been built to validate the ground model. A schematic of the apparatus is illustrated in Figure 2. In this setup an inner copper tube with an external diameter of 22 mm (0.75 in.) is placed at the geometric center of a sand-filled cylinder. A solution of water/ethylene glycol (50%) is pumped through the inner tube from the bottom.

The cylinder is filled with so-called Ottawa sand (C-109). This laboratory-grade sand is frequently used as a test sample. Detailed information on the physical characteristics and thermal properties of this sand has been reported by Tarnawski et al. (2009, 2011). The sand is fully saturated with water and tests are performed below and above the freezing temperature of water to validate the model in melting/solidification cycles.

The temperature in the sand is measured using 16 type T calibrated thermocouples. As shown in Figure 2, the thermocouples are staggered radially and placed along four azimuthal positions. The position uncertainty of all the temperature measurements made in the sand is estimated at ±1 mm (0.04 in.).

In the first part of the validation, the inlet temperature of the fluid to the inner pipe was set to a constant value of –20°C (–4°F) for the first 3.5 h in order to freeze the saturated sand around the inner tube. Then, as shown in Figure 3a, the fluid temperature was varied above and below the freezing point to simulate melting and solidification cycles. As shown in Figure 3a, the temperature evolutions of the three measuring points located 25, 35, and 75 mm (1, 1.25, and 3 in.) from the center are different. Points further from the center experience dampened oscillations that are shifted in time. At the end of the first heat extraction cycle (at t = 3.5 h), calculated temperatures of the first and third thermocouples reach –6.1°C (21°F) and –1.0°C (30°F), respectively. This indicates that they are both located in the frozen region. The numerical model agrees with these experimental results within the experimental uncertainty. At t = 3.5 h, the inner wall temperature is increased. As shown in the zoomed portion in Figure 3b, the temperature of the frozen region (represented here by TC1) increases gradually up to –0.2°C (31.6°F), close to the melting point. The temperature remains constant from t = 3.54 to 3.62 h as the region melts. The

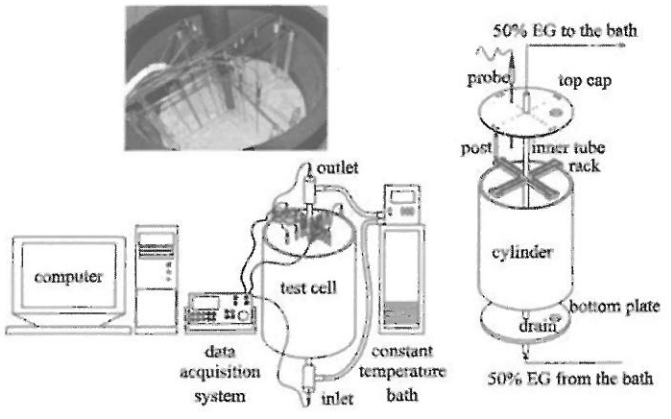

Figure 2 *Experimental setup used for validation.*

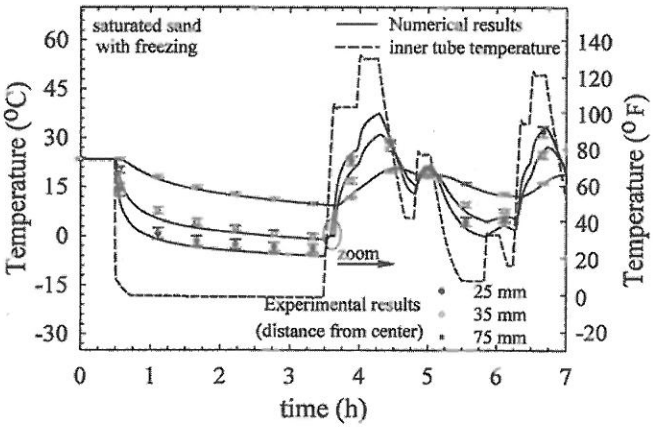

(*a*)

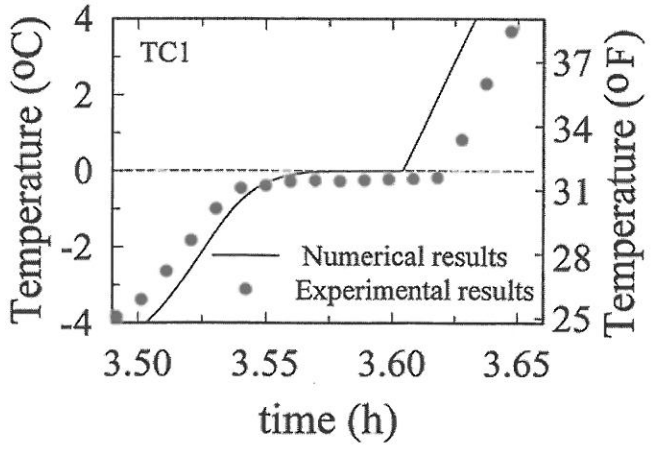

(*b*)

Figure 3 *Temperature evolution of saturated sand at different locations under freezing conditions.*

numerical model was able to capture this plateau. Overall, these results show that the numerical model can be considered to be validated. More validation results can be found in the study performed by Eslami-nejad and Bernier (2012).

SIMULATIONS

Configurations

GCHP system simulations are carried out over an entire year to examine the merits of the PCM-sand ring configuration. Two alternatives are compared and are shown in Figure 4 with characteristics given in Table 1.

Case 1, which is used as the reference case, represents a conventional GCHP system with a single U-tube borehole. Case 2 is a single U-tube borehole surrounded by a relatively small PCM-sand ring. Both boreholes are equipped with two 3.34 cm (1.3 in.) diameter pipes and the grout thermal conductivity is set at 2.5 $W \cdot m^{-1} \cdot K^{-1}$(1.44 $Btu \cdot h^{-1} \cdot ft^{-1} \cdot °F^{-1}$). In Case 1, both pipes are positioned with a center-to-center distance ($2D$) of 7.5 cm (2.95 in.) inside a borehole with a radius, r_b = 7.5 cm (2.95 in.). In Case 2, pipes are in intimate contact ($2D$ = 4.1cm [1.61 in.]) inside a borehole with a 4.1cm (1.61 in.) radius. A PCM ring with a thickness ($r_r - r_b$) set at 3.4 cm (1.34 in.) is added giving an overall diameter of 15 cm (6 in.), which is the same as in Case 1. For Case 2, the ring would have to be contained in some form of casing. In this study, it is assumed that the thickness of this casing is negligible and that the PCM ring is in direct contact with the grout at r_b = 4.1 cm (1.61 in.) and with the ground at r_r = 7.5 cm (2.95 in.). The PCM ring thickness initially selected proved to be insufficient during peak conditions. As shown later, additional simulations were performed to find an optimum radius that would minimize borehole length.

Borehole and Ground Models Integration

Following the two-region approach proposed by Yang et al. (2009), the ground and borehole models are coupled at the borehole wall as shown in Figure 5. An iterative solution is used at each time step to link the borehole and ground models: the iteration starts by guessing a value of T_b. Then, the heat transfer rate at the borehole wall, q_b, is calculated using the borehole model developed by Zeng et al. (2003). Next, the ground model, which extends from the borehole wall to the far-field, uses this value of q_b to calculate a new value of T_b. Calculations continue until the difference between two successive T_b values drop below the convergence criteria.

Table 1. Borehole Characteristics

Borehole Configuration	r_b	r_p	$2D$	r_r	k_{grout}
	cm (in.)				$W \cdot m^{-1} \cdot K^{-1}$ ($Btu \cdot h^{-1} \cdot ft^{-1} \cdot °F^{-1}$)
Case 1	7.5 (2.95)	1.67 (0.66)	7.5 (2.95)	—	2.5 (1.44)
Case 2	4.1 (1.61)	1.67 (0.66)	4.8 (1.89)	7.5 (2.95)	2.5 (1.44)

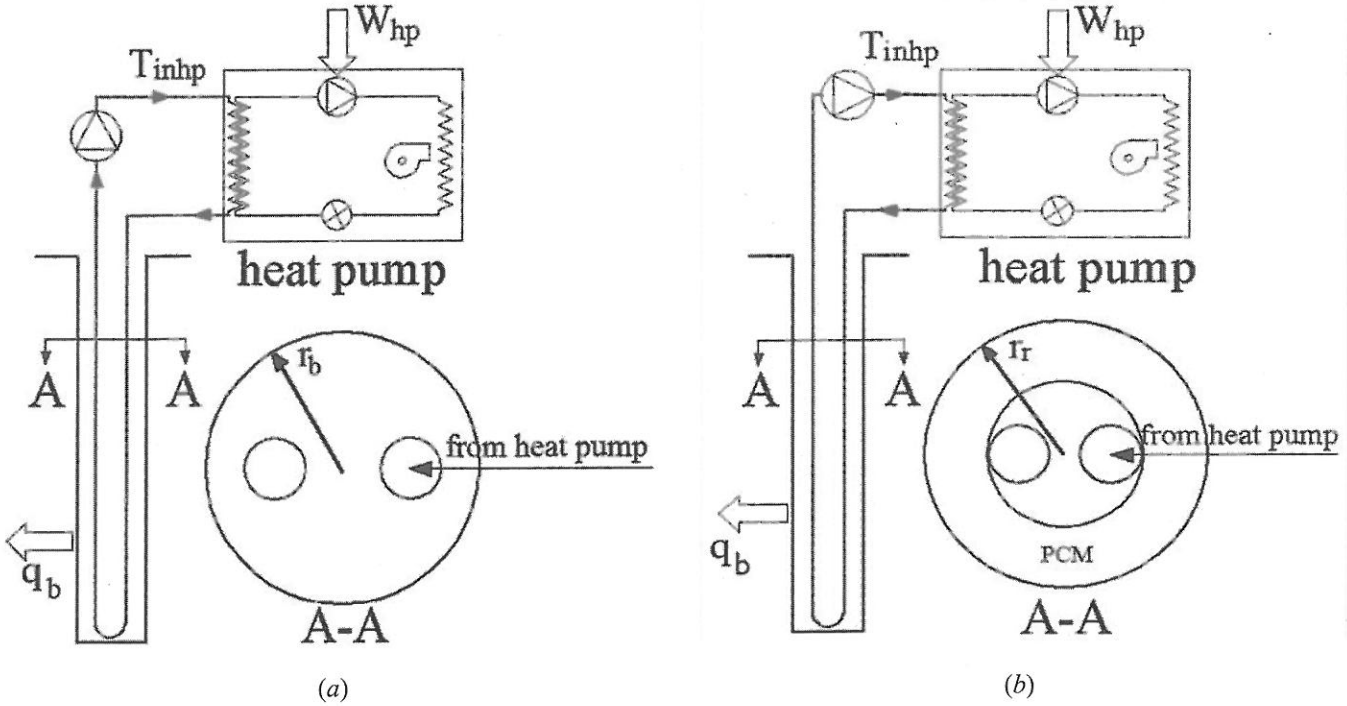

Figure 4 Schematic representations of Cases 1 and 2.

Characteristics of the PCM ring

In cooling mode, the ground loops usually work in the 20°C to 40°C (68°F to 104°F) temperature range. Therefore, the PCM needs to be selected to work at these temperatures. Salt hydrates and organic PCMs are both available in this range of melting temperature (Pcmproducts 2012). However, both have relatively low thermal conductivities. In this work, the PCM is mixed with Ottawa sand C-109 to increase the thermal conductivity of the ring. The sand is composed of subrounded quartz grains with a solid cube thermal conductivity of 7.59 $W \cdot m^{-1} \cdot K^{-1}$ (4.39 $Btu \cdot h^{-1} \cdot ft^{-1} \cdot °F^{-1}$) and a thermal diffusivity (with a porosity of 36%) of 0.0198 $m^2 \cdot day^{-1}$ (0.213 $ft^2 \cdot day^{-1}$) (Tarnawski et al. 2009, 2011).

The resulting effective thermal conductivity (k_{eff}) of the PCM-sand mixture is evaluated using the experimentally validated analytical correlation derived by Reddy and Karthikeyan (2011). Based on this correlation, the geometry of the medium is considered to be composed of a matrix of touching and nontouching in-line solid and hollow cubes. The ratio of the effective thermal conductivity over the PCM thermal conductivity, K, is given by:

$$K = \frac{k_{eff}}{k_f} = \left[\frac{1-\varepsilon}{1+\varepsilon^2\psi^2(\alpha-1)} + \frac{\varepsilon(1-\psi)}{1+\varepsilon^2(\alpha-1)} + \frac{\varepsilon\psi}{(2\varepsilon\psi - 2\varepsilon^2\psi + \varepsilon^2)(\alpha-1)+1} \right]^{-1} \quad (5)$$

where $\varepsilon = 0.1$ and $\Psi = 0.86$ are length and contact ratios, respectively, while α is the ratio of the solid cube thermal conductivity of the sand over the PCM thermal conductivity (k_f).

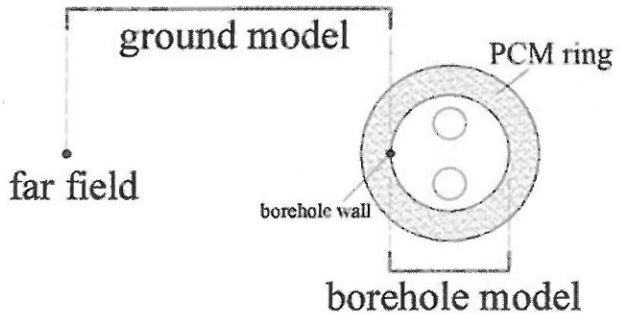

Figure 5 *Borehole and ground model calculation domains.*

A variety of PCMs are available. Table 2 summarizes the characteristics of salt hydrates and organic PCM for a melting temperature of 32°C (89.6°F).

Based on the data reported in Table 2, salt hydrate PCMs have a higher latent heat capacity and thermal conductivity than organic PCMs and will therefore be used in this study. Using Equation 5, the effective thermal conductivity of the PCM-sand mixture is 2.5 $W \cdot m^{-1} \cdot K^{-1}$ (1.44 $Btu \cdot h^{-1} \cdot ft^{-1} \cdot °F^{-1}$) while the thermal diffusivity is 0.095 $m^2 \cdot day^{-1}$ (1.02 $ft^2 \cdot day^{-1}$).

In order to restrict the analysis to the impact of the PCM ring, the ground-thermal conductivity and diffusivity are set at the same values. For the same reason, the grout thermal conductivity for both cases is also set to 2.5 $W \cdot m^{-1} \cdot K^{-1}$ (1.44 $Btu \cdot h^{-1} \cdot ft^{-1} \cdot °F^{-1}$). Finally, the effects of air gaps that may be introduced over time due to the expansion/contraction of the PCM are not considered in the present study.

Building load

The building used in this study is a well-insulated 150 m^2 (1650 ft^2) residence located in Miami, Florida in a hot and humid climate. The annual building load was obtained using a TRNSYS simulation. The heating and cooling setpoints were set at 20°C and 25°C (68°F and 77°F), respectively. The resulting building load profile is shown in Figure 6.

As shown in Figure 6, the peak space heating and cooling loads are 4.5 kW (15,350 Btu/h) and 9.8 kW (33,440 Btu/h), respectively. The annual space cooling requirement over the cooling season (April to December) is 16,285 kWh (55.57 × 10^6 Btu) while the annual space heating requirement is 314 kWh (1.07 × 10^6 Btu).

Heat Pump

This building is air-conditioned with a 3-ton (10.5 kW) single-capacity heat pump. The cooling capacity is sufficient to cool the building at peak conditions with an EFT of 20°C (68°F). Figure 7 shows the heat pump capacity and compressor power for both cooling and heating modes as a function of the heat pump inlet temperature.

The building load and the heat pump performance are used along with the combined borehole/PCM ring ground models in annual simulations. A 6-minute time step was used with the heat pump being either on or off during the 6-minute time step depending on whether the building load had been met. Finally, the undisturbed far-field ground temperature is assumed to be 20°C and corresponds to ground temperatures in Miami, Florida.

Table 2. ***Thermal Properties of Two Types of PCM for a Melting Temperature of* 32°C (89.6°F)**

PCM	Latent Heat Capacity $kJ \cdot kg^{-1}$ ($Btu \cdot lb^{-1}$)	Specific Heat Capacity $kJ \cdot kg^{-1} \cdot K^{-1}$ ($Btu \cdot lb^{-1} \cdot °F^{-1}$)	Thermal Conductivity k_f ($W \cdot m^{-1} \cdot K^{-1}$) ($Btu \cdot h^{-1} \cdot ft^{-1} \cdot °F^{-1}$)	Density $kg \cdot m^{-3}$ ($lb \cdot ft^{-3}$)
Salt Hydrate	200 (86)	1.91 (0.46)	0.51 (0.29)	1460 (91)
Organic	130 (56)	2.2 (0.53)	0.21 (0.12)	845 (53)

RESULTS AND DISCUSSION

Several preliminary simulations were undertaken to find which PCM melting temperature would lead to the shortest borehole in Case 2. Among the salt hydrate PCMs offered by one manufacturer (Pcmproducts 2012), the one with a melting temperature of 32°C (89.6°F) led to the shortest borehole. The required borehole length was determined by trial and error through several annual simulations. It was selected so as to keep T_{inhp} below 38°C (100°F) at all times during the cooling season while satisfying the building loads in both the cooling and heating seasons.

Results, including required borehole length (H), building load (q_{build}), cumulative heat pump energy consumption (W_{hp}) both in winter and summer, extracted energy from the ground (q_b) in winter, injected energy to the ground (q_b) in summer, and finally seasonal (winter and summer) averages of inlet temperature to the heat pump ($\overline{T_{inhp}}$) are presented in Table 3. This table is divided into two parts. The second and third columns present the results for cases 1 and 2 while the last column presents results for case 2 but with an optimum PCM ring radius.

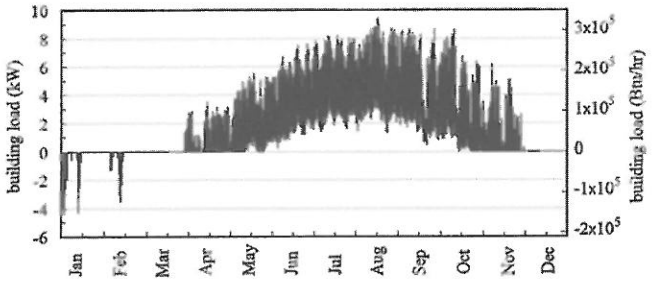

Figure 6 *Building load used in the present study.*

As shown in Table 3, the required borehole length for case 1 is 192 m (630 ft) while the corresponding value for Case 2 is 178 m (584 ft), a reduction of 7.3%. In winter, the heat pump extracts 238 kWh (0.81×10^6 Btu) from the ground and uses 76 kWh (0.26×10^6 Btu) for the compressor (W_{hp}) to provide the required heating load (q_{build}) of 314 kWh (1.07×10^6 Btu). It is interesting to note that these results are identical for both cases. The borehole in Case 1 is longer which leads to a higher average inlet temperature to the heat pump, 16.6°C (61.9°F), compared to Case 2, 16.2°C (61.2°F). However, this small difference has an insignificant impact on heat pump energy consumption. The situation is somewhat different for the summer results. As shown in Table 3, for Case 1, the heat pump rejects annually 24,893 kWh (84.93×10^6 Btu) to the ground (q_b) and uses 8608 kWh (29.37×10^6 Btu) for the compressor (W_{hp}) to provide the required cooling load (q_{build}) of 16285 kWh (55.57×10^6 Btu)

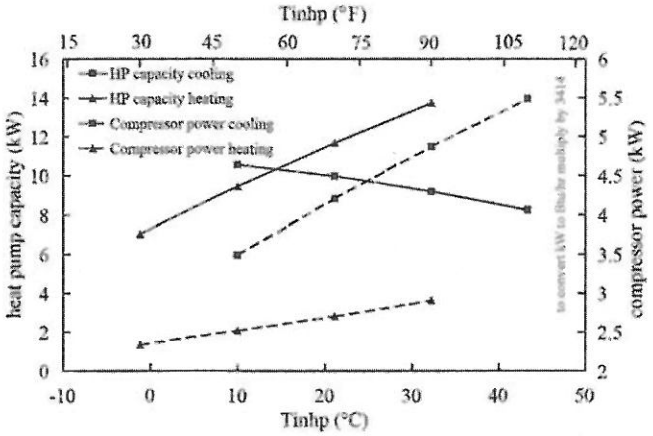

Figure 7 *Heat pump capacity and corresponding compressor power requirement as a function of the heat pump inlet temperature.*

Table 3. Results of Annual Simulations

		Case 1	Case 2	Case 2 Optimum
	Ring Radius, cm (in.)	—	7.5 (2.95)	8.5 (3.35)
	H, m (ft)	192 (630)	178 (584)	174 (571)
Winter	q_{build}, kWh (Btu)		314 (1.07×10^6)	
	W_{hp}, kWh (Btu)	76 (0.26×10^6)	76 (0.26×10^6)	76 (0.26×10^6)
	q_b, kWh (Btu)	–238 (-0.81×10^6)	–238 (-0.81×10^6)	–238 (-0.81×10^6)
	$\overline{T_{inhp}}$ °C (°F)	16.6 (61.9)	16.2 (61.2)	16.1 (61.2)
Summer	q_{build}, kWh (Btu)		16,285 (55.56×10^6)	
	W_{hp}, kWh (Btu)	8608 (29.37×10^6)	8780 (29.96×10^6)	8845 (30.18×10^6)
	q_b, kWh (Btu)	24,893 (84.93×10^6)	25,065 (85.52×10^6)	25,130 (85.74×10^6)
	$\overline{T_{inhp}}$ °C (°F)	31.7 (89.1)	32.6 (90.7)	33.0 (91.4)

For Case 2, 25,065 kWh (85.52×10^6 Btu) of energy is rejected into the ground by the heat pump, a marginal 0.7% increase when compared to Case 1. Similarly, the heat pump energy consumption (W_{hp}) is increased by 2% (from 8607 to 8780 kWh [29.37×10^6 to 29.96×10^6 Btu]). Using a shorter borehole in Case 2 raises the average inlet fluid temperature to the heat pump. The summer average values of $\overline{T_{inhp}}$ for Cases 1 and 2 are 31.7°C (89.1°F) and 32.6°C (90.7°F), respectively. This results in a slight increase in heat pump energy consumption. It is worth mentioning that the higher value of W_{hp} in Case 2 might be partially compensated by the fact that less pumping energy is required to overcome a reduced pressure drop in shorter boreholes.

For Case 2, there are occasions during the summer when the 3.4 cm (1.34 in.) ring is completely melted. In such cases, the advantage offered by the PVM ring no longer exists and the EFT increases if heat rejection continues. Another set of simulations was performed with an optimum PCM thickness. This optimum was selected so that melting occurs at least once at the outer PCM ring radius during the cooling season. As shown in the last column of Table 3, the resulting optimum radius is 8.5 cm (3.35 in.). Using this radius, the required borehole length is 174 m (571 ft), an 18 m (59 ft) reduction (9.3%) when compared to Case 1, while a 2.7% increase in the heat pump energy consumption is observed when compared to Case 1. This is due to the higher average inlet temperature (33.0°C [91.4°F] in Case 2 Optimum and 31.7°C [89.1°F] in Case 1). It should be noted that a further increase in the ring thickness did not lead to a reduction of the required borehole length.

Figure 8 presents the annual variations of the borehole wall temperature (T_b) and of the inlet temperature to the heat pump (T_{inhp}). The full set of Case 2 results are presented. However, for Case 1, only values that exceed the Case 2 results at specific times are presented. Finally, results are presented only when the heat pump is operating.

Figure 9 indicates the radial location of the melted interface for Case 2. An overlay of a borehole section is shown on the left of the figure to illustrate the relative location of the ring. In both figures, results are presented for the entire year. However, the discussion below focuses on the cooling season, from April to December.

As shown in Figure 8 for Case 2, T_b and T_{inhp} increase over time as the heat pump rejects heat into the ground. At the beginning of July, T_b reaches the melting temperature 32°C (89.6°F) and melting of the PCM ring starts. As indicated in Figure 9, the thickness of the melted portion of the ring progresses until it reaches the value of the ring thickness in mid-August. At that point the PCM ring is entirely melted.

It remains entirely melted for about five hours during this peak cooling load condition. During that short period, no further melting occurs, heat transfer is by pure conduction, and the borehole wall temperature, T_b, will rise above 32°C (89.6°F) for a few hours. As the cooling season progresses, the building load decreases and heat pump operation is infrequent. The neighbouring ground (the far-field is at 20°C [68°F]) cools the ring and the melted interface position moves towards the borehole radius, r_b. However, this process is insufficient to solidify the whole ring and T_b does not fall below 32°C (89.6°F) until about mid-October when the building load becomes small. Thus, from July to mid-October the borehole temperature, T_b, oscillates but does not often go above 32°C (89.6°F), the melting temperature of the PCM ring. Also, as shown in Figure 8, T_{inhp} remains below 37°C (98.6°F) most of the time. Finally, as the building load is reduced further, T_b and T_{inhp} decrease due to the net heat flow to the far-field from the borehole.

For Case 1, as shown in Figure 8, T_b and T_{inhp} values are higher than for Case 2 only during peak conditions (from July to mid-October). At other times, the values of T_b and T_{inhp} are lower for Case 1. This can be explained by the fact that the longer borehole in Case 1 leads to lower temperatures when

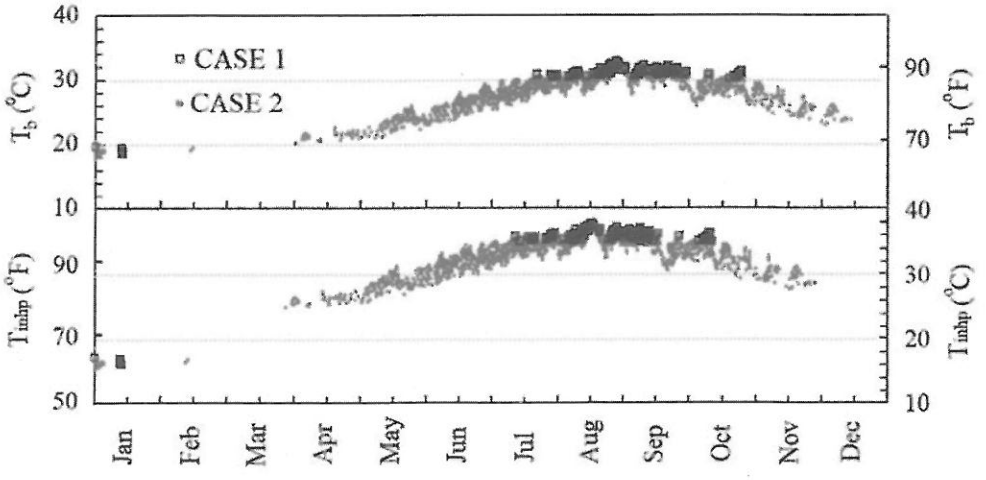

Figure 8 T_b *and* T_{inhp} *for Cases 1, and 2.*

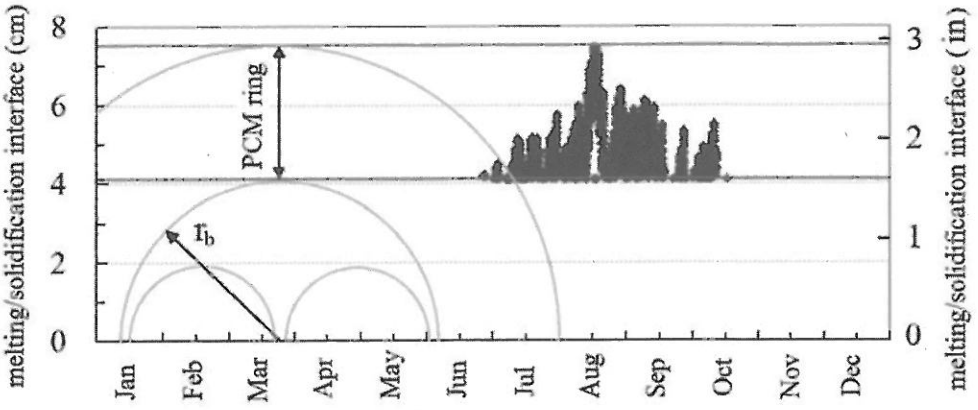

Figure 9 *Melting/solidification interface for Case 2.*

there is no melting. However, when the melting starts, T_b remains at 32°C (89.6°F) in Case 2, while it continues to increase above 32°C (89.6°F) in Case 1.

CONCLUSIONS AND RECOMMENDATIONS

A new borehole configuration is proposed in this study in an attempt to reduce the required length of GHEs in residential applications. It consists of a single U-tube borehole surrounded by a ring made of a mixture of PCM and sand. In cooling mode, the PCM-sand ring is allowed to melt during peak load conditions to take advantage of the relatively high energy content associated with the latent heat of fusion of the PCM.

A 1-*D* radial numerical heat transfer model is developed to evaluate heat transfer from the borehole wall to the far-field. The model accounts for multiple radial layers and phase changes are handled using the effective capacity method. It is shown that the results of the numerical model are in very good agreement with experimental results obtained on a small scale set up equipped with saturated (with water) sand.

Several annual simulations were undertaken to examine the merits of the proposed borehole configuration in a cooling-dominated climate. A typical residential building located in Miami, Florida equipped with a 3-ton heat pump is used. The peak building load is 9.8 kW (33,440 Btu/h), and the annual space building requirement is 16,285 kWh (55.57×10^6 Btu). A 6-min. time step was used with the heat pump being either on or off during the time step depending on whether the building load had been met.

Results show that for configurations with a PCM-sand ring, the borehole wall temperature remains around 32°C (89.6°F), the melting temperature of the selected PCM, for several hours during peak cooling conditions, while the borehole wall temperatures increase to higher temperatures for regular boreholes. When a PCM-sand ring with a thickness of 3.4 cm (1.34 in.) is used, results show that the borehole length can be reduced by about 7.3% for this particular case with a marginal 2% increase in the heat pump energy consumption. However, this thickness is not optimum as it does not offer enough latent heat potential at peak conditions. If the thickness of the PCM-sand ring is increased to 4.1 cm (1.61 in.) such that melting does not go beyond the ring radius at peak conditions, then the borehole length can be reduced by 9.3% with a corresponding increase in the heat pump energy consumption of 2.7% when compared to a regular borehole. These are relatively promising results based on one particular case. More simulations to cover various peak conditions and ground conditions are required to ascertain the full potential of this new configuration.

The numerical model presented here is based on a number of assumptions, including 1-*D* radial heat transfer. A 2*D* model (radial-azimuthal) model along with a full-scale experimental validation is under development.

ACKNOWLEDGEMENTS

The financial support provided by CanmetENERGY-Varennes and the NSERC Smart Net Zero Energy Buildings Strategic Network is gratefully acknowledged.

NOMENCLATURE

1-*D*	= one-dimensional
2*D*	= center-to-center distance between pipes, m (ft)
k_{eff}	= effective thermal conductivity of the PCM-sand mixture, $W \cdot m^{-1} \cdot K^{-1}$ ($Btu \cdot h^{1} \cdot ft^{-1} \cdot °F^{-1}$)
k_f	= thermal conductivity of the PCM, $W \cdot m^{-1} \cdot K^{-1}$ ($Btu \cdot h^{1} \cdot ft^{-1} \cdot °F^{-1}$)
k_{grout}	= grout thermal conductivity, $W \cdot m^{-1} \cdot K^{-1}$ ($Btu \cdot h^{1} \cdot ft^{-1} \cdot °F^{-1}$)
k_r	= PCM ring thermal conductivity, $W \cdot m^{-1} \cdot K^{-1}$ ($Btu.h^{-1} \cdot ft^{1} \cdot °F^{-1}$)
$\dot{m}$	= mass flow rate of the circulating fluid, $kg \cdot s^{-1}$ ($lb \cdot s^{-1}$)
q_b	= extracted or injected energy from/to the ground, kWh (Btu)
q_{build}	= building load, kWh (Btu)

r_b = borehole radius, m (ft)

r_p = pipe external radius, m (ft)

r_r = PCM ring radius, m (ft)

T_b = borehole wall temperature, °C (°F)

T_{inhp} = inlet fluid temperature to the heat pump, °C (°F)

W_{hp} = annual heat pump energy consumption, kWh (Btu)

ϕ = sand porosity

ρc = heat capacity, $J \cdot m^{-3}$ ($Btu \cdot ft^{-3}$)

REFRENCES

Allan, M.L. and S.P. Kavanaugh. 1999. Thermal conductivity of cementitious grouts and impact on heat exchanger length design for ground source heat pumps. *HVAC&R Research* 5(2):85–96.

Bernier, M. and A. Salim Shirazi. 2007. Solar heat injection into boreholes: a preliminary analysis. *Proceeding of 2nd Canadian Solar Building Conference,* Calgary, Canada, T1-1-1:8 pages.

Bonacina, C., G. Comini, A. Fasano, and M. Primicerio. 1973. Numerical solution of phase-change problems. *International Journal of Heat and Mass Transfer* 16(10):1825–32.

Chiasson, A.D., and C. Yavuzturk. 2003. Assessment of the viability of hybrid geothermal heat pump systems with solar thermal collectors. *ASHRAE Transactions* 109(2):487–500.

Chiasson, A.D., and C. Yavuzturk. 2009. A design tool for hybrid geothermal heat pump systems in heating-dominated buildings. *ASHRAE Transactions* 115(2):1–13.

Eslami-nejad, P., and M. Bernier. 2011a. Coupling of geothermal heat pumps with thermal solar collectors using double U-tube borehole with two independent circuits. *Applied Thermal Engineering* 31(14–15):3066–77.

Eslami-nejad, P., and M. Bernier. 2011b. Heat transfer in double U-tube boreholes with two independent circuits. *ASME Journal of Heat Transfer* 133(8):1–12.

Eslami-nejad, P., and M. Bernier. 2012. Freezing of geothermal borehole surroundings: A numerical and experimental assessment with application. *Applied Energy* 98:333–45.

Eslami-nejad, P., A. Langlois, S. Chapuis, M. Bernier, and W. Faraj. 2009. Solar heat injection into boreholes. *Proceeding of 4th Canadian Solar Building Conference*, Toronto, Canada:237–246.

Hackel, S., G. Nellis, and S. Klein. 2009. Optimization of cooling-dominated hybrid ground-coupled heat pump systems. *ASHRAE Transactions* 115(1): 565–80.

Kjellsson, E., G. Hellström, and B. Perers. 2010. Optimization of systems with the combination of ground-source heat pump and solar collectors in dwellings. *Energy* 35(6):2667–73.

Patankar, S.V. 1980. *Numerical Heat Transfer And Fluid Flow*, 2nd Ed., New York: McGraw-Hill.

Pcmproducts. 2012. www.pcmproducts.net.

Reddy, K.S., and P. Karthikeyan. 2009. Estimation of effective thermal conductivity of two-phase materials using collocated parameter model. *Heat transfer engineering* 30(12):998–1011.

Remund, C.P. 1999. Borehole thermal resistance: Laboratory and field studies. *ASHRAE Transactions* 105(1):1–7.

Raymond, J., M. Frenette, A. Léger, E. Magni, and R. Therrien. 2011. Numerical modeling of thermally enhanced pipe performances in vertical ground heat exchangers. *ASHRAE Transactions* 117(1):1–9.

Tarnawski V.R., T. Momose, and W.H. Leong. 2011. Thermal conductivity of standard sands II. Saturated Conditions. *International Journal of Thermophysics* 32(5):984–1005.

Tarnawski V.R., T. Momose, W.H. Leong, G. Bovesecchi, and P. Coppa. 2009. Thermal conductivity of standard sands—Part I: Dry-state conditions. *International Journal Of Thermophysics* 30(3):949–68.

Xi, C., L. Lin, and Y. Hongxing. 2011. Long term operation of a solar-assisted ground coupled heat pump system for space heating and domestic hot water. *Energy and Buildings* 43(8):1835–44.

Yang, H., P. Cui, and Z. Fang. 2010. Vertical-borehole ground-coupled heat pumps: A review of models and systems. *Applied Energy* 87 (1):16–27.

Yang, W., M. Shi, G. Liu, and Z. Chen. 2009. A two-region simulation model of vertical U-tube ground heat exchanger and its experimental verification. *Applied Energy* 86(10):2005–12.

Yavuzturk, C., and J.D. Spitler. 2000. Comparative study of operating and control strategies for hybrid ground-source heat pump systems using a short time step simulation model. *ASHRAE Transactions* 106(2):192–209.

Zeng, H., N. Diao, and Z. Fang. 2003. Heat transfer analysis of boreholes in vertical ground heat exchangers. *International Journal of Heat and Mass Transfer* 46(23):4467–81.